Synthesis and characterization of CuO nanofibers, and investigation for its suitability as blocking layer in ZnO NPs based dye sensitized solar cell and as photocatalyst in organic dye degradation

R. Sahay [a], J. Sundaramurthy [a], P. Suresh Kumar [a], V. Thavasi [b,*], S.G. Mhaisalkar [a], S. Ramakrishna [b,*]

[a] School of Materials Science and Engineering, Nanyang Technological University, 50 Nanyang Avenue, Singapore 639798, Singapore

[b] NUS Nanoscience and Nanotechnology Initiative, National University of Singapore, Singapore 117576, Singapore

**Corresponding authors. Fax: +65 6872 5563. E-mail addresses: velnanotech@gmail.com (V. Thavasi),seeram@nus.edu.sg (S. Ramakrishna).*

Abstract

Electrospun copper based composite nanofibers were synthesized using the copper acetate/polyvinyl alcohol/water solution as starting material. Synthesized composite nanofibers were sintered at 500 ℃ to obtain CuO nanofibers. XRD, FTIR and XPS techniques were used to confirm the presence of pure CuO nanostructures. The effect of annealing cycle on the crystalline structure of the CuO nanofibers was analyzed and observed that the decrease in crystallite size with an increase in the dwelling time improved the orientation of the CuO crystallite. The blue-shift in the band-gap energies of CuO nanofibers was observed as a result of quantum confinement from bulk CuO (1.2 eV) to one dimensional (1D) nanostructures (~1.746 eV). The catalytic activity of the CuO fibers for the degradation of methyl orange was carried out and as a blocking layer in ZnO based DSSC was fabricated and observed a 25% increase in the current density.

Keywords: Copper oxide; Nanofibers; Electrospinning; DSSC; Catalysis Band-gap

1. Introduction

Transition metal oxides nanostructures have been widely used due to their unique features such as high specific surface area, chemical stability and electrochemical activity at nanoscale with promising applications in applied science and technology. Among various transition metal oxides, copper based oxides such as cuprous oxide (Cu_2O) and cupric oxide (CuO) has lot of significant properties, which need to be explored. Cu_2O is widely employed in energy applications due to its high charge mobilities [1]; whereas, research is on-going to employ CuO p-type semiconductor with a narrow band-gap of E_g=1.2 eV, in energy applications due to its high carrier concentration [2]. It has been widely noted that the chemical and physical properties of copper oxides can be changed either by changing the fabricating process or the process parameters [3]. One of the most analyzed process parameter is the post annealing temperature, which can alter the oxidation states of copper resulting in the variation of the physical and chemical properties. Figueiredo et al. [4] observed an increase in the optical band-gap with the increase in the post annealing temperature of the as-deposited Cu films. On the other hand, Xi et al. [5] observed a change in the morphology of CuO from microspheres to nanowires with the increase in the process temperature of the hydrothermal method. Only few works have been performed to monitor the changes in the physical and chemical properties with the changes in the dwelling time of the annealing process. Therefore, an attempt was made to analyze the growth mechanism of the CuO crystallite with the dwelling time such as 4, 6, 8 and 12 h, respectively.

Although many techniques such as chemical vapor deposition (CVD) [6], hydrothermal [7], sol–gel [8] and electrochemical deposition [9] have already been used for the fabrication of CuO with various morphologies, research is on-going on a reliable and economic process for the production of large-scale high-quality CuO nanomaterials due to their applicability in various technological areas such as as-catalysis [10], batteries [11], solar energy conversion [12], gas sensing [13] and field emission applications [7]. Recently, it has been observed that the re-exploration of 1D-nanostructure production

technique known as electrospinning, due to its simplicity and uniqueness of producing high aspect ratio nanofibers. This technique involves preparation of a sol–gel with the compatible inorganic precursor and polymer dissolved in a particular solvent. The technical details about the effect of processing as well as system parameters on electrospinning technique can be seen elsewhere [14, 15]. These nanofibers were found to be of great significance because of their inherent property such as large surface area and the engineered property such as porosity.

Majority of transition metal oxides are being employed for the photo-catalytic activities such as TiO_2, SnO_2, ZnO, Fe_2O_3, CuO, etc. Nevertheless, CuO has been scarcely employed as a photocatalyst to degrade organic pollutants such as textile dyes, due to its inability to produce good amount of OH• radicals. This phenomenon may be the result of fast electron/hole recombination and the position of the valence band edge of CuO with respect to the redox potential necessary for the generation of OH• [16]. Yu et al. [3] observed that a CuO thin film depicts no photo-catalytic activity under visible-light irradiation, unless H_2O_2 is added as one of the sources of OH•. They found that the presence of CuO complimented H_2O_2 for an improved degradation of methyl orange dye. The other approach includes fabrication of composite nanomaterials employing CuO as one of the ingredients to improve the overall catalytic activity. These configurations include CuO/TiO_2 [17], CuO/ZnO [18], CuO/X zeolite [19], etc. In this report, photo-degradation of methyl orange was carried out under UV irradiation employing CuO nanofibers as the catalyst, thus completely eliminating H_2O_2 or composite counterpart, thus paving the way for stable and affordable photocatalyst. It was noted that 60% of the dye degraded within 1 h of exposure to the UV radiation in the presence of CuO nanofibers. Kim et al. [20] observed that the high conduction band edge of the blocking layer can retard the back transfer of electrons from the photoanode to the electrolytes or the dye. The usage of CuO nanofibers as the blocking layer in ZnO based dye sensitized solar cells (DSSCs) is also analyzed as it has high conduction band edge as compared to ZnO.

2. Materials and methods

Copper acetate (99%), zinc acetate (99%), polyvinyl alcohol PVA (M_W=80,000–124,000) and 100% pure acetic acid were purchased from Aldrich and used as received without any further purification. 0.5 g Of the copper acetate ($Cu(CH_3COO)_2 \cdot H_2O$) was dissolved in 4.5 ml of 10 wt% aqueous PVA solution. This solution was then stirred for 24 h at room temperature for the formation of pale blue colored copper hydroxide. Eq. (1) represents the chemical reaction depicting the hydrolysis of the employed precursor to the formation of $Cu(OH)_2$. Later, as-prepared solution was introduced in 10 ml syringe with a hypodermic needle (*dia.* 27G) in a controlled electrospinning setup (ELECTROSPUNRA, Singapore).

$$Cu(CH_3COO)_2 \cdot H_2O + H_2O \xrightarrow{\text{yields}} Cu(OH)_2 + 2CH_3COOH. \quad (1)$$

The flow rate and applied electric filed was varied to obtain the optimal conditions for the electrospun fibers. The obtained optimal condition was as follows: flow rate of 0.2 ml/h and the applied electric field of 1.25 kV/cm. High electric field strength (1.4 kV/cm) was employed to enable for the high stretch rates of the electrospun jet. The distance between the needle tip and the collector against the applied electric field was set as 18 cm. The longer distance between the needle tip and the collector aided the stretching of the jet due to the increase in the distance covered by the spiraling electrospun jet before being deposited on the collector. The fiber mesh obtained was then annealed to obtain CuO nanofibers. Annealing of the electrospun fibers at 500 °C for 4, 6, 8 and 12 h caused the elimination of water molecules from the copper hydroxide and resulted in the formation of cupric oxide (CuO) as given in Eq. (2). The heating and cooling rates employed were kept constant at 2 and 5 °C/min, respectively,

$$Cu(OH)_2 \xrightarrow{\Delta} H_2O + CuO. \quad (2)$$

2.1.Synthesis of ZnO nanoparticles for photoanode

DSSC was constructed using ZnO as the photo-electrode. ZnO nanoparticles were prepared by sol–gel technique by using equimolar zinc acetate and sodium hydroxide

(NaOH). The mixed aqueous solution was stirred using a magnetic stirrer at room temperature until a clear white solution was obtained. The clear white solution thus obtained was refluxed at 80 °C for 4 h and then allowed to cool down to room temperature. The as-prepared ZnO powder samples were subjected to calcination in a muffle furnace at 250 °C for 1 h. Finally, the calcinated white ZnO powder was obtained after gradual cooling down to room temperature.

2.2.DSSC fabrication

Fluorine doped indium oxide (FTO) (2.0 cm x 1.5 cm; 15 Ω/cm^2, Asahi Glass Co. Ltd., Japan) substrates were first cleaned in a detergent solution using an ultrasonic bath for 20 min and then rinsed with water and ethanol successively and dried at 80 °C in an oven. Typically, 0.25 g of prepared ZnO nanoparticles was ultrasonically dispersed in 0.6 mL of acetic acid (99%) for 20 min. Further, 0.1 g of polyethylene glycol (M_W=100,000) was added as the binder and allowed to agitate for 2 h. As-prepared ZnO paste was coated on to the cleaned FTO substrates using doctor blade technique to an average thickness of 20 μm. The dispersion of CuO nanofibers in deionised water (5 mg/ml) is then spin-coated on top of the ZnO layer to form a blocking layer having an average thickness of 1 μm. The substrate was then heated at 500 °C for 1 h under the normal atmosphere to remove the binder. Two different dyes were employed to visualize their effect on the performance of the solar cell. These dyes include Eosin-Y and Ru based N719 dye. The as-prepared ZnO photo-electrode with area of 0.28 cm^2 was soaked in a given dye for 24 h at the ambient temperature. The dye-anchored electrode was then washed in ethanol to remove unbound dye and dried under vacuum for 15 min, and was sealed using a 30 μm thick spacer. These photo-electrodes were then sandwiched with Pt coated on the conducting substrate (FTO) as the counter electrode to complete the device as shown in Fig. 1. Electrolyte containing 0.1 M lithium iodide, 0.03 M iodine, 0.5 M 4-tert-butylpyridine and 0.6 M 1-propyl-2, 3-dimethyl imidazolium iodide in acetonitrile solvent was filled in the device.

2.3.Characterization

A PANanalytical (XPERT-PRO) X-ray diffractometer using $CuK\alpha_1$ radiation (λ=1.5406 Å) was employed to characterize the crystallographic properties of the post-annealed CuO nanofibers samples. The surface morphologies of the samples were characterized by a scanning electron microscopy (SEM, JEOL JSM). Photocurrent measurements were carried out using a solar simulator (XES-151S, San Ei, Japan) under AM 1.5 G condition. UV–vis spectral analysis was recorded on Shimadzu UV-3150. XPS measurements were made on a Kratos Analytical AXIS HSi spectrometer with a monochromatized AlKα X-ray source (1486.71-eV photons) at a constant dwell time of 100 ms and pass energy of 40 eV. The core-level signals were obtained at a photoelectron takeoff angle of 90° (with respect to the sample surface). The X-ray source was run at a reduced power of 150 W. The pressure in the analysis chamber was maintained at 7.5×10^{-9} Torr or lower during each measurement. FT-IR analysis was performed by AVATAR 360, Fourier Transforms Infrared spectroscope.

3. Results and discussion

3.1.Surface and structural analysis

SEM image of the composite CuO/ PVA nanofibers and annealed CuO nanofibers for 12 h is shown in Fig. 2(a) and (b). It can be seen from the SEM images that a random mesh of nanofibers was obtained. This randomness of the fiber mesh obtained was the direct consequence of the bending instability associated with the electrospun jet [21]. The distribution of annealed CuO fibers soaked at 12 h was found to be around 141±54 nm whereas 269±76 nm represent the distribution of composite CuO/PVA fibers. This reduction of CuO fiber diameter upon annealing was due to the removal of residual polymer as carbon dioxide and water vapor. The composite fiber mesh obtained was then annealed at 500 °C in the air for 4, 6, 8 and 12 h. The heating and cooling rates employed were kept constant at 2 and 5 °C /min, respectively. Finally, annealing of the composite fibers resulted in the formation of poly-crystalline CuO structure with predominate (111)

phase orientation. During the analysis, no appreciable change in the morphology of the CuO nanofibers was observed with the dwelling time from 4 to 12 h.

XRD analysis performed at different dwelling times with the other parameters kept constant is shown in the Fig. 3(a). All the diffraction peaks at 2θ= 32.54°, 35.54°, 38.70°, 48.77°, 53.48°, 58.29°, 61.65°, 66.28° and 68.14° were purely assigned to the (110), (002), (111), (-202), (020), (202), (-113), (-311), (220) crystal planes, respectively. It can be seen that all the diffraction peaks belong to the CuO monoclinic phase (JCPDS 48-1548) with lattice constant of *a*= 0.4598 nm, *b*=0.346 nm and *c*=0.523 nm. Compared to the standard diffraction patterns, there were no characteristic peaks from impurities, such as $Cu(OH)_2$ or Cu_2O, indicating that $Cu(OH)_2$ was completely transformed into CuO after annealing. It was also noted that the reflections of (111) orientation was the strongest, suggesting as the preferential crystal planes of the CuO nanofibers. Broadening of the diffraction peaks with the increase in the dwelling time resulted in the reduction of the crystallite size of CuO nanofibers as observed in Fig. 3(b). The average crystallite sizes of these post-annealed samples were calculated from the peak widths using the following Scherrer equation

$$D = \frac{0.94\lambda}{\beta \cos\theta} \tag{3}$$

whereas the relationship for strain is

$$\varepsilon = \frac{\beta \cot\theta}{4} \tag{4}$$

where, D is the crystallite size, λ is the wavelength (1.546 Å for Cu Ka), β is the full-width at half-maximum (FWHM) of main intensity peak after subtraction of the equipment broadening and θ is the diffraction angle. The lattice strain of the (111) orientated CuO nanofibers prepared at the different dwelling time are shown in Fig. 3(b) was calculated using the Eq. (4). As expected, the lattice strain increased with the decrease in the crystallite size leading to the improved orientation of CuO crystallites. XRD pattern of the synthesized ZnO powder samples showed the well-crystalline wurtzite ZnO phases. All the diffraction peaks orientated along (100), (002), (101), (102), (110), (103), (200), (112), (201), (004), (202) correspond to the pure ZnO phase (JCPDS Card No. 36–1451) as observed from Fig. 4(a) and corre-sponding SEM image typically

shows the formation of spherical ZnO nanoparticles with the diameter ranging from 100 nm to 150 nm confirmed from the inset in Fig. 4(b).

3.2.Chemical composition analysis

XPS is a powerful technique for analyzing the chemical composition of elements on the surface of compounds and studying the transition metal compounds having the localized valence *d* orbitals. The detailed XPS analysis confirmed the formation of CuO nanofibers, which are shown in Fig. 5(a)–(c). The peaks at 932.8 eV and 953.1 eV confirmed the presence of Cu $2p_{3/2}$ and Cu $2p_{1/2}$ peaks, respectively (Fig. 5(a)). Along with the main peak at 932.8 eV, the shake-up satellite peaks were observed at the higher binding energy side, 934.3 eV, 940.6 eV and 943.1 eV (Fig. 5(b)). The main peak was characteristic of Cu^{+}, whereas the shake-up satellite peaks were characteristics of partially filled d-block ($3d^{9}$) of $Cu^{2+.}$ The peak positions and relative intensities of the satellites against the core levels were indicative of the formation of CuO particles. The detailed XPS analysis of O 1s is shown in Fig. 5(c). The main peak at 529.5 eV corresponds to O 1s of CuO. This particular O 1s peak accounting for 60% of the total spectral area confirming Cu–O bonds, whereas the left-over portion of the total spectral area can be associated with $(OH)_2$ groups (530.5–531.6 eV) and oxygen defective sites (531.6 eV) [22]. Ratio of the sum of the peak areas of Cu^{2+} and Cu^{+} were performed to measure their relative amount on the surface, and it suggested that some reduction of Cu^{2+} to Cu state [23]. This reduction of Cu^{2+} to Cu^{+} can be due to a group of reasons such as, (a) exposure to X-ray during the acquisition of XPS data [23], (b) the presence of carbon obtained during the treatment of these substrates in the air, (c) it was argued that the acetic acid formed during the hydrolysis of copper acetate (Eq. (1)) can act as a reducing agent. This reducing agent may be the reason for the phase transformation of CuO to Cu_2O as shown in [3] depicted by Eq. (5).

$$8CuO + CH_3COOH \xrightarrow{\text{yields}} 4Cu_2O + 2CO_2 + 2H_2O \qquad (5)$$

As the CuO crystallite size decreased with an increase in the dwelling time, the relative amount of Cu^{+}/Cu^{2+} increased. This increase in the relative amount of Cu^{+} with

respect to Cu^{2+} can be attributed to the increased reduction by X-ray exposure due to the decrease in the particle size. The decrease in the particles size results in the increase of the surface to the volume ratio, which results in the increase of the amount of atoms available on the surface for the reduction to Cu^{+}. It was also observed that the binding energy of the Cu $2p_{3/2}$ line and the characteristic area ratio decreased with the increase in the particle size. This phenomenon may be due to an increase in the bond ionicity associated with the reduction in the co-ordination number induced by the particle size reduction down to the nanometer scale and the resulting narrowing of the electron energy levels. FTIR analysis was performed to confirm the presence of characteristic vibrational peaks pertaining to CuO nanofibers as shown in Fig. 6. The wavenumbers positioned at 531 cm^{-1} (4 h) and 533 cm^{-1} (6, 8 and 12 h) correspond to Cu–O stretching vibrations. The wavenumbers at 487 cm^{-1} (4 h), 484 cm^{-1} (6 h), 481 cm^{-1} (8 h) and 483 cm^{-1} (12 h) represented the other characteristic peaks re-confirming the poly-crystalline nature of CuO nanofibers [24]. Weak bands at 2926 cm^{-1} (4 h), 2926 cm^{-1} (6 h), 2917 cm^{-1} (8 h) and 2919 cm^{-1} (12 h) were assigned to alkyl (sp^3) (C–H) stretching. The corresponding CH_2 bend occurred at 1405 cm^{-1} (4 h), 1404 cm^{-1} (6 h), 1399 cm^{-1} (8 h) and 1400 cm^{-1} (12 h). Weak peaks were also observed at 1632 cm^{-1} (4 h), 1633 cm^{-1} (6 h), 1629 cm^{-1} (8 h) and 1629 cm^{-1} (12 h) correspond to frequency against stretching of C=C bond. These week peaks may correspond to impurities present on the surface of the nanofibers during measurement.

3.3.Effect of crystalline size on the band-gap

UV–vis analysis was performed to investigate the optical properties of the CuO nanofibers as a function of the dwelling time. The thin film samples for UV–vis analysis were prepared by using spin-coating techniques at 1000 rpm for 30 s on the glass substrate. These thin films were prepared from the CuO nanofibers dispersed in deionised water (5 mg/ml). The band-gap energies of the CuO nanofibers were found to be of the order of 1.7 eV. The band-gap energy of bulk CuO is estimated to be in the range of 1.2–1.5 eV [25]. The blue-shift observed in the band-gap can be attributed to the result of quantum confinement usually observed in 1D nanostructure [26]. It was noted that the

band-gap of the nanofibrous sample increased with an increase in the dwelling time as seen in Fig. 7. The band-gap energy values as a function of dwelling time are 1.746 (4 h), 1.769 (6 h), 1.771 (8 h) and 1.771 (12 h). The obtained result complies with the effective mass theory (EMA), which predicts r^{-2} dependence of the band-gap, with r^{-1} correction term in the strong confinement regime, where r is the crystallite size. As mentioned earlier, the crystallite size decreases with the increase in the dwelling time resulting in the increase in the band-gap energy according to the effective mass theory (EMA).

4. Applications of CuO nanofibers

4.1.Dye degradation with CuO as photocatalyst

Cu^{2+} in CuO has a partially empty d and s block, which increases its affinity for the available free electrons and thus making it a good p type material. Whereas, Cu^{+} has only empty s block achieves better charge transfer density in comparison to Cu^{2+}. This is due to the strong affinity for electron by the empty d block in case of Cu^{2+}. The research has been on-going globally to employ Cu^{2+} in applications such as catalysis due to its high carrier concentration [1]. In our present study, highly crystalline CuO nanofibers obtained at dwelling time of 12 h were used for photocatalysis. Methyl orange (4-dimethylaminoazobenzene-4'-sulfonic acid sodium salt—$C_{14}H_{14}N_3NaO_3S$) was chosen for the analysis as it is being widely employed in textile industry, making it as a classic case-study material. 10^{-5} M of dye solution was prepared in deionized water. UV–vis analysis was performed on dye solution to obtain the maxima pertaining to the dye, which was found to be 464 nm. Dye to the catalyst concentration ratio was kept as 1:10 for the analysis. The methyl orange solution with CuO nanofibers was stirred for 12 h and then degraded by placing it under a 4 W UV lamp. In aqueous dye solutions the holes (h^{+}) were scavenged by surface hydroxyl groups to generate the oxidizing hydroxyl radical (OH•) and electrons (e^{-}) were scavenged by oxygen groups to generate the O_2^- radical to promote the oxidation of dye. UV light has energy ranges between 1.24 and 3.1 eV, which is more than the energy required for the primary reaction as methyl orange energy band-gap is 2.6 eV. CuO nanofibers as photocatalyst accelerated the degradation of dye

on virtue of its small band-gap (1.77 eV), which enhanced the creation of e^-/h^+ pair. We observed 60% of the dye decomposition within 1 h of UV illumination as shown in Fig. 8. A similar study was performed by employing CuO thin films as the catalyst under UV irradiation for the degradation of methyl blue [16]. Nevertheless, low-level degradation of the methyl blue was observed due to the scarcity of the OH• radicals. It is argued that the large surface area and oriented crystallites of CuO nanofibers resulted in the improved degradation of the dye in the present analysis.

4.2.Device performance

The preliminary analysis of DSSC employing CuO as a blocking layer was presented. The photocurrent densities versus photo-voltage (J–V) characteristic are shown in Fig. 9. The resultant photovoltaic parameters such as open-circuit voltage (V_{oc}), short-circuit current density (J_{sc}), fill factor (FF) and the conversion efficiency are summarized in Table 1. CuO nanofibers obtained at 12 h dwelling time were employed as a blocking layer because of its improved orientation that resulted from its small crystallite size. We observed the increase in photocurrent with the incorporation of CuO nanofibers as a blocking layer. The retardation of the interfacial recombination by the CuO blocking layer was the reason for the reduction in the reverse current thus improving the current density. This phenomenon was possible as the conduction band edge of CuO is situated above ZnO creating a potential gradient, which allowed the forward movement of electron leading to the low reverse current. The inverse of the slope at the V_{oc} to the (J–V) characteristic curve is proportional to the series resistance of the cell. This series resistance was a function of metal contact resistance and the resistance to the flow of electron through the dye to the FTO attached to ZnO. It was noted that the inverse of the slope at the V_{oc} decreases with the incorporation of CuO blocking layer, particularly for N719 dye implying the reduction of series resistance. Similarly, R_{sh} represents the obstruction to an alternate path for the flow of current, which can be deduced by inverse of the slope at the I_{sc}. High value of R_{sh} implied that the series resistance was the major reason for lower current density. As expected, the highest current density was obtained for the cells having lower series resistance. Lower series resistance was realized by

incorporating CuO as a blocking layer which restricted the recombination electron–hole pairs leading to relatively high current density. The difference in the current density for N719 and Eosin-Y can be explained on the basis of carboxylate anchoring group. The carboxylate anchoring group was the cause for the grafting of the sensitizer on to the ZnO surface [27]. Two carboxylate anchoring groups in N719 compared to one for Eosin-Y resulted in improved grafting of sensitizer and thus resulted in the improved current density for N719 dye. Work is still in the process to further improve the efficiency of solar cells and analyze the scattering nature of the poly-crystalline CuO nanofiber blocking layer.

5. Conclusions

The effect of the dwelling time of the annealing cycle for the formation of the crystallite CuO nanofibers was analyzed. It was observed that the crystallite size of CuO nanofibers decreased with an increase in the dwelling time. This decrease in the crystallite size resulted in the improved orientation of the CuO nanofibers. The highly ordered morphology obtained at 12 h was employed for photo-catalytic study. It was noted that 60% of the organic dye was decomposed within 1 h of UV illumination. Preliminary results based on the study on the suitability of CuO nanofibers as the blocking layer in ZnO based DSSC was also presented. A 25% increase in the current density was observed with the application of CuO as blocking layer. We have hereby fabricated highly crystalline CuO nanofibers with possible energy applications.

Acknowledgements

This work was supported by Singapore NRF-CRP grant on “Nanonets for Harnessing Solar Energy and Storage” and also NUS and NTU for providing facilities to carry out the research. Dr. V. Thavasi acknowledges NUSNNI for support.

References

[1] J.R. Hayes, G.W. Nyce, J.D. Kuntz, J.H. Satcher, A.V. Hamza, Nanotechnology 18 (2007) 275602.

[2] A.H. Jayatissa, K. Guo, A.C. Jayasuriya, Appl. Surf. Sci. 255 (2009) 9474–9479.

[3] H.G. Yu, J.G. Yu, S.W. Liu, S. Mann, Chem. Mater. 19 (2007) 4327–4334.

[4] V. Figueiredo, E. Elangovan, G. Gonc-alves, N. Franco, E. Alves, S.H.K. Park, R. Martins, E. Fortunato, Phys. Status Solidi A 206 (2009) 2143–2148.

[5] Y. Xi, C. Hu, P. Gao, R. Yang, X. He, X. Wang, B. Wan, Mater. Sci. Eng. B 166 (2009) 113–117.

[6] T. Maruyama, Sol. Energy Mater. Sol. Cells 56 (1998) 85–92

[7] M.A. Dar, Y.S. Kim, W.B. Kim, J.M. Sohn, H.S. Shin, Appl. Surf. Sci. 254 (2008) 7477–7481.

[8] S.C. Ray, Sol. Energy Mater. Sol. Cells 68 (2001) 307–312.

[9] L. Chen, S. Shet, H.W. Tang, H.L. Wang, T. Deutsch, Y.F. Yan, J. Turner, M. Al Jassim, J. Mater. Chem. 20 (2010) 6962–6967.

[10] P. Bera, A.L. Camara, A. Hornes, A. Martinez-Arias, J. Phys. Chem. C 113 (2009) 10689–10695.

[11] M.A. Dar, S.H. Nam, Y.S. Kim, W.B. Kim, J. Solid State Electrochem. 14 (2010) 1719–1726.

[12] K.P. Musselman, A. Wisnet, D.C. Iza, H.C. Hesse, C. Scheu, J.L. MacManus¬Driscoll, L. Schmidt-Mende, Adv. Mater. 22 (2010) E254–258.

[13] J.J. Chen, K. Wang, L. Hartman, W.L. Zhou, J. Phys. Chem. C 112 (2008) 16017–16021.

[14] D.H. Reneker, A.L. Yarin, Polymer 49 (2008) 2387–2425.

[15] C.J. Thompson, G.G. Chase, A.L. Yarin, D.H. Reneker, Polymer 48 (2007) 6913–6922.

[16] M. Miyauchi, A. Nakajima, T. Watanabe, K. Hashimoto, Chem. Mater. 14 (2002) 2812–2816.

[17] G.H. Li, N.M. Dimitrijevic, L. Chen, T. Rajh, K.A. Gray, J. Phys. Chem. C 112 (2008) 19040–19044.

[18] B. Rohe, R. Weiss, S. Vukojevic, C. Baltes, M. Muhler, M. Tausch, M. Epple, Eur. J. Inorg. Chem. (2007) 1723–1727.

[19] A. Nezamzadeh-Ejhieh, S. Hushmandrad, Appl. Catal. A 388 (2010) 149–159.

[20] J.Y. Kim, S. Lee, J.H. Noh, H.S. Jung, K.S. Hong, J. Electroceram. 23 (2009) 422–425.

[21] D.H. Reneker, A.L. Yarin, H. Fong, S. Koombhongse, J. Appl. Phys. 87 (2000) 4531–4547.

[22] S.J. Stewart, M. Multigner, J.F. Marco, F.J. Berry, A. Hernando, J.M. Gonzalez, Solid State Commun. 130 (2004) 247–251.

[23] Y. Iijima, N. Niimura, K. Hiraoka, Surf. Interface Anal. 24 (1996) 193–197.

[24] G. Kliche, Z.V. Popovic, Phys. Rev. B 42 (1990) 10060–10066.

[25] T. Ito, H. Yamaguchi, K. Okabe, T. Masumi, J. Mater. Sci. 33 (1998) 3555–3566.

[26] J. Tang, L. Brzozowski, D.A.R. Barkhouse, X.H. Wang, R. Debnath, R. Wolowiec, E. Palmiano, L. Levina, A.G. Pattantyus-Abraham, D. Jamakosmanovic, E.H. Sargent, ACS Nano 4 (2010) 869–878.

[27] M. Gratzel, MRS Bulletin 30 (2005) 23–27.

List of Tables

List of Figures

W UV lamp under ambient conditions, i.e. 295 K and relative humidity (RH), 60% air.

Fig. 9 Photocurrent density–voltage characteristics of DSSCs.

Configuration	V_{oc} (mV)	J_{sc} (mA/cm^{-2})	FF	Efficiency (%)
FTO/ZnO/N719/ electrolyte/Pt	0.399	0.643	0.381	0.098
FTO/ZnO/**CuO**/N719/ electrolyte/Pt	0.439	0.787	0.439	0.152
FTO/ZnO/Eosin-Y/ electrolyte/Pt	0.283	0.089	0.512	0.013
FTO/ZnO/**CuO**/Eosin-Y/electrolyte/Pt	0.332	0.092	0.609	0.019

Table 1

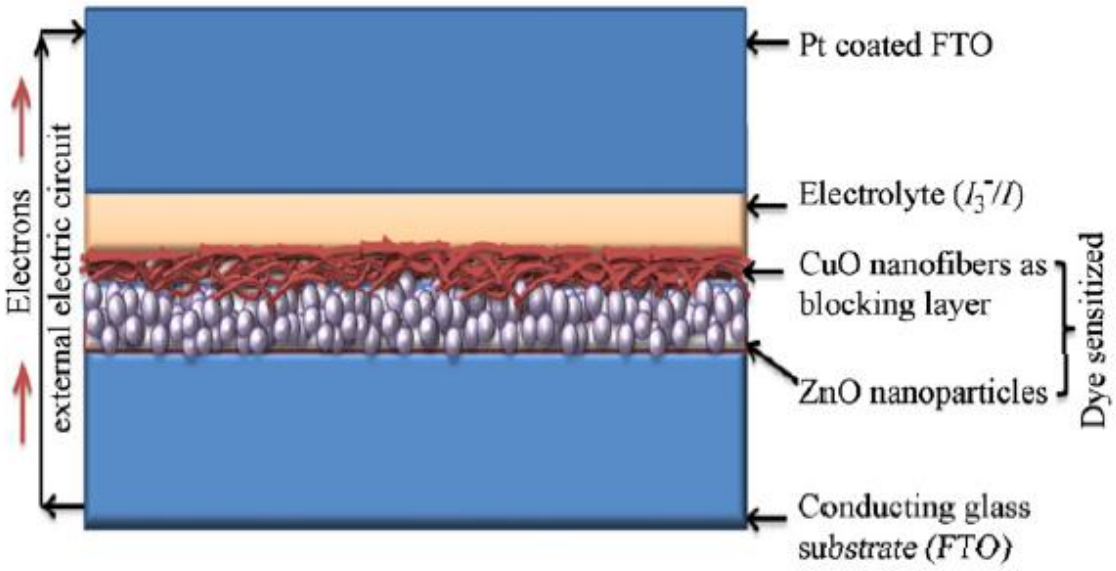
Pt coated FTO
Electrolyte (I_3^-/I)
CuO nanofibers as blocking layer
ZnO nanoparticles
Dye sensitized
Conducting glass substrate (FTO)
Electrons
external electric circuit

Fig. 1

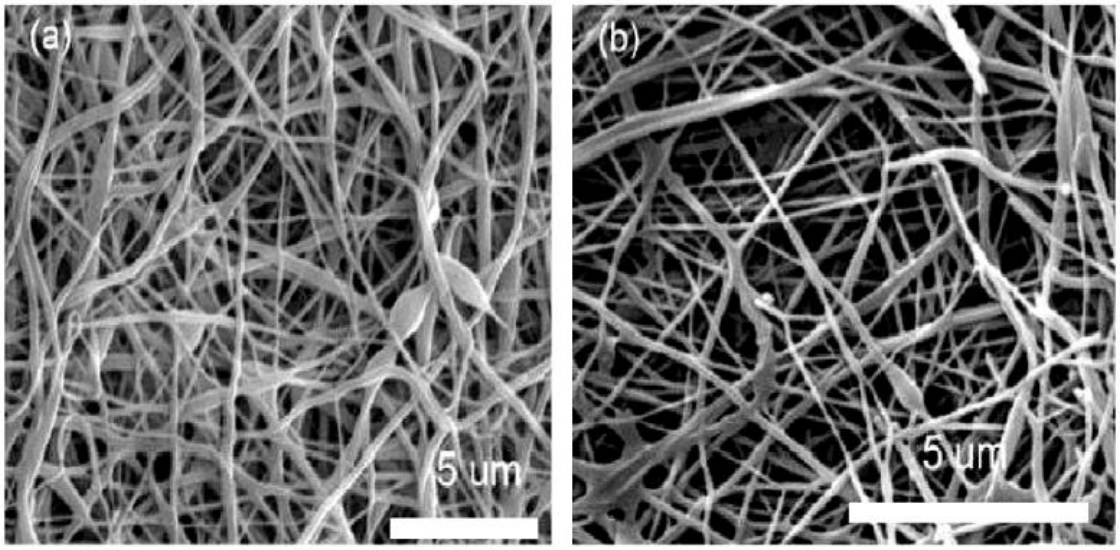

Fig. 2

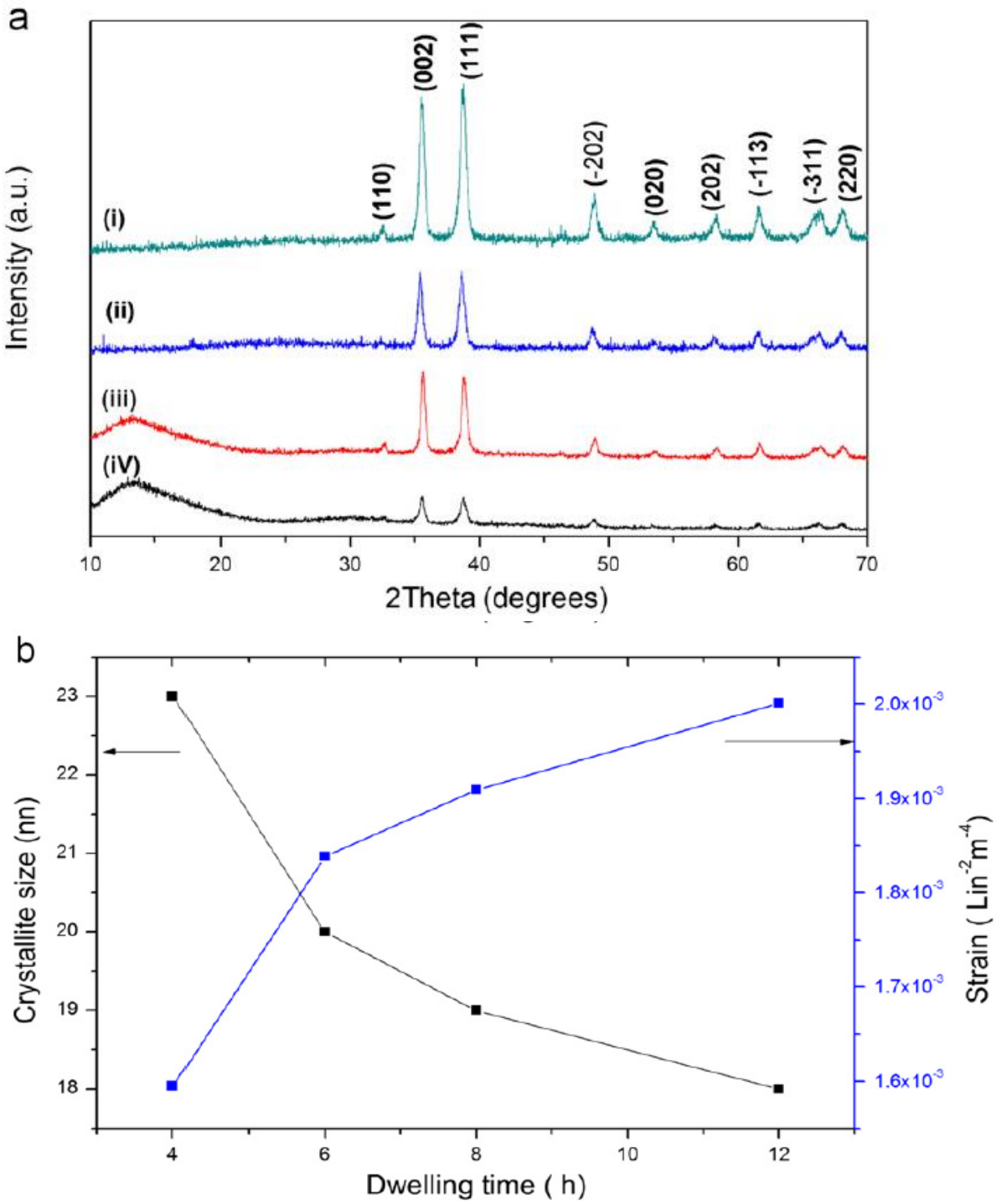
a
Intensity (a.u.)
(i)
(ii)
(iii)
(iV)
(110)
(002)
(111)
(-202)
(020)
(202)
(-113)
(-311)
(220)
10
20
30
40
50
60
70
2Theta (degrees)
b
Crystallite size (nn)
Strain (Lin^{-2}m^{-4})
18
19
20
21
22
23
1.6x10^{-3}
1.7x10^{-3}
1.8x10^{-3}
1.9x10^{-3}
2.0x10^{-3}
4
6
8
10
12
Dwelling time (h)

Fig.3

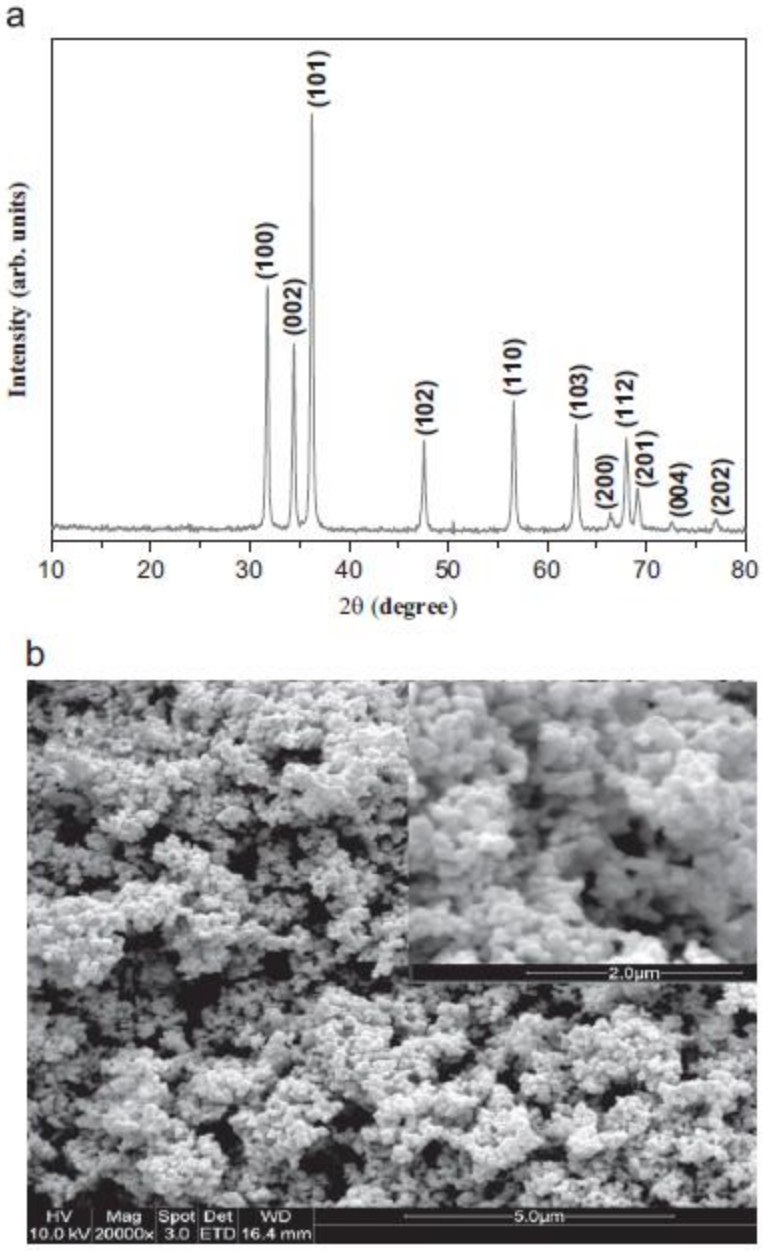
a
Intensity (arb. units)
(100)
(002)
(101)
(102)
(110)
(103)
(200)
(112)
(201)
(004)
(202)
10
20
30
40
50
60
70
80
2θ (degree)
b
2.0μm
HV
Mag
Spot
Det
WD
10.0 kV
20000x
3.0
ETD
16.4 mm
5.0μm

Fig. 4

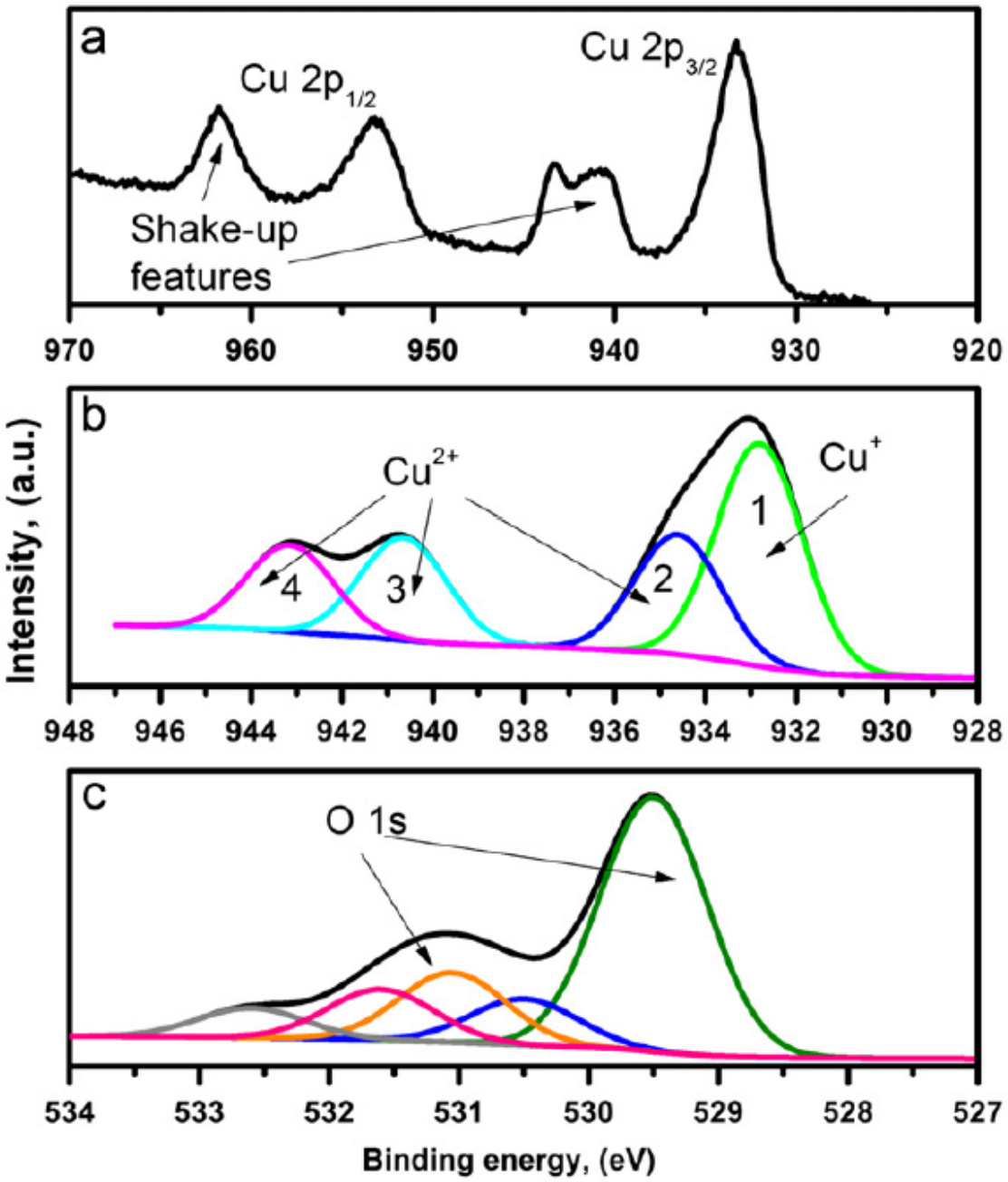
a
Cu 2p1/2
Cu 2p3/2
Shake-up
features
970
960
950
940
930
920
b
Cu2+
Cu+
1
2
3
4
Intensity, (a.u.)
948
946
944
942
940
938
936
934
932
930
928
c
O 1s
534
533
532
531
530
529
528
527
Binding energy, (eV)

Fig. 5

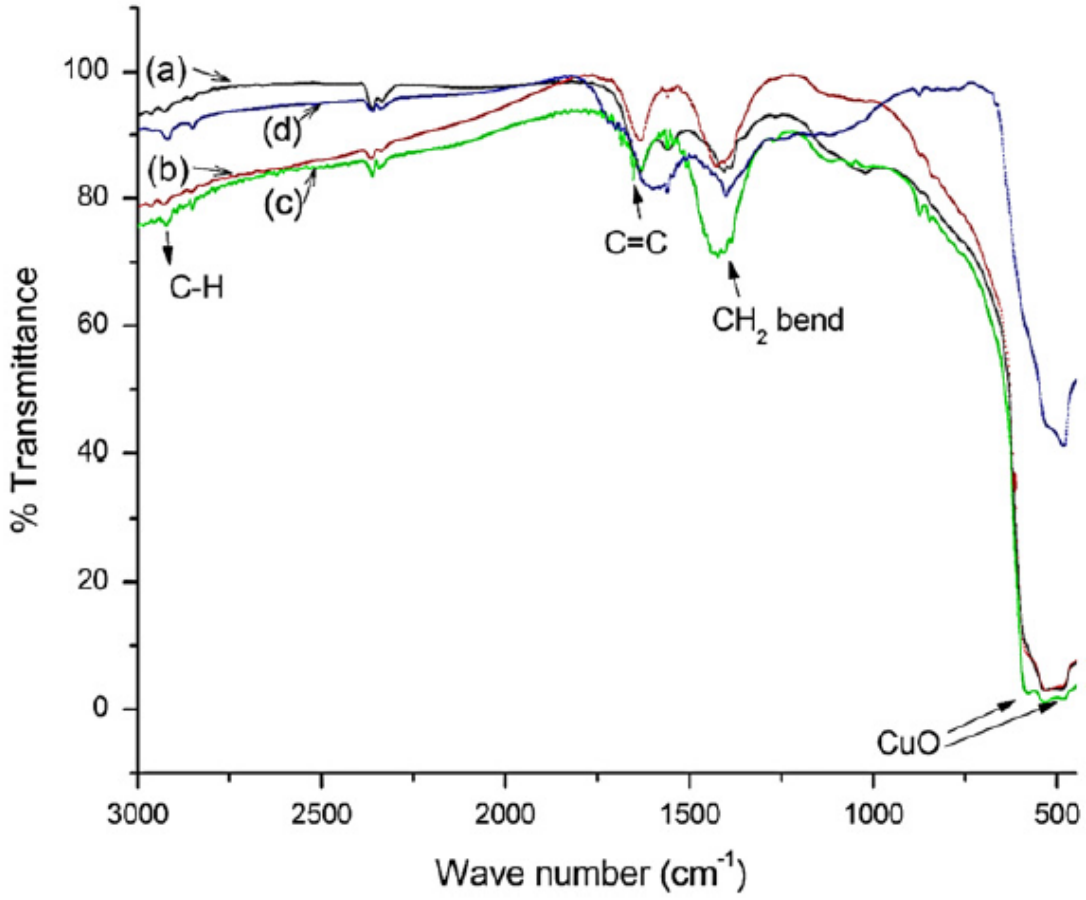
(a)
(d)
(b)
(c)
C-H
C=C
CH2 bend
CuO
% Transmittance
Wave number (cm-1)
100
80
60
40
20
0
3000
2500
2000
1500
1000
500

Fig. 6

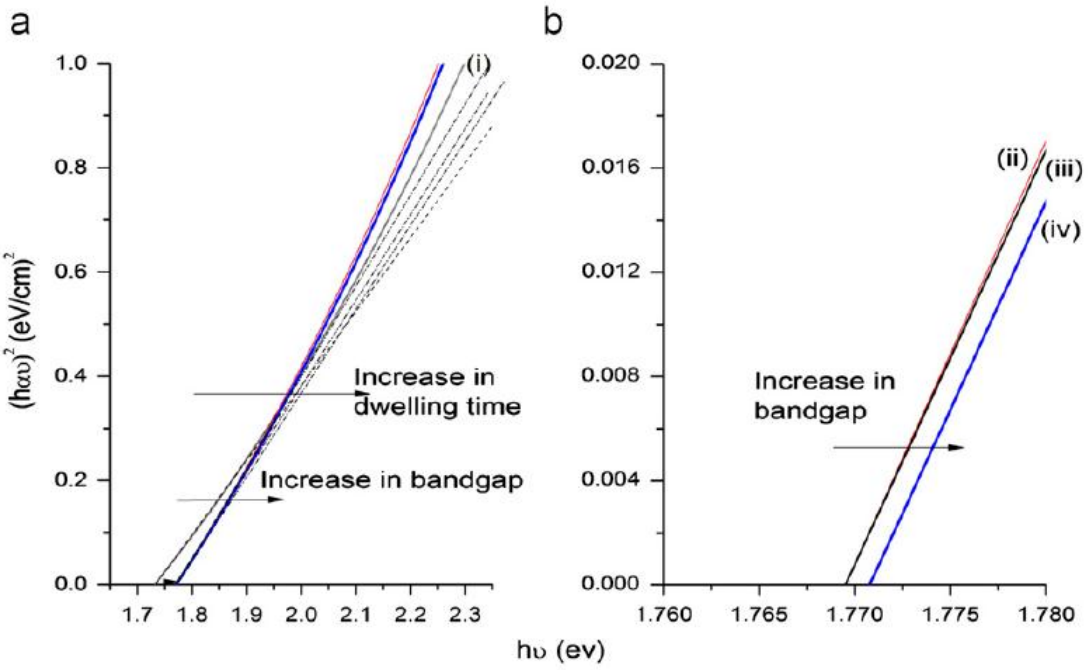
a
b
1.0
0.8
0.6
0.4
0.2
0.0
(hω)² (eV/cm)²
(i)
Increase in
dwelling time
Increase in bandgap
1.7
1.8
1.9
2.0
2.1
2.2
2.3
0.020
0.016
0.012
0.008
0.004
0.000
(ii)
(iii)
(iv)
Increase in
bandgap
1.760
1.765
1.770
1.775
1.780
hυ (ev)

Fig. 7

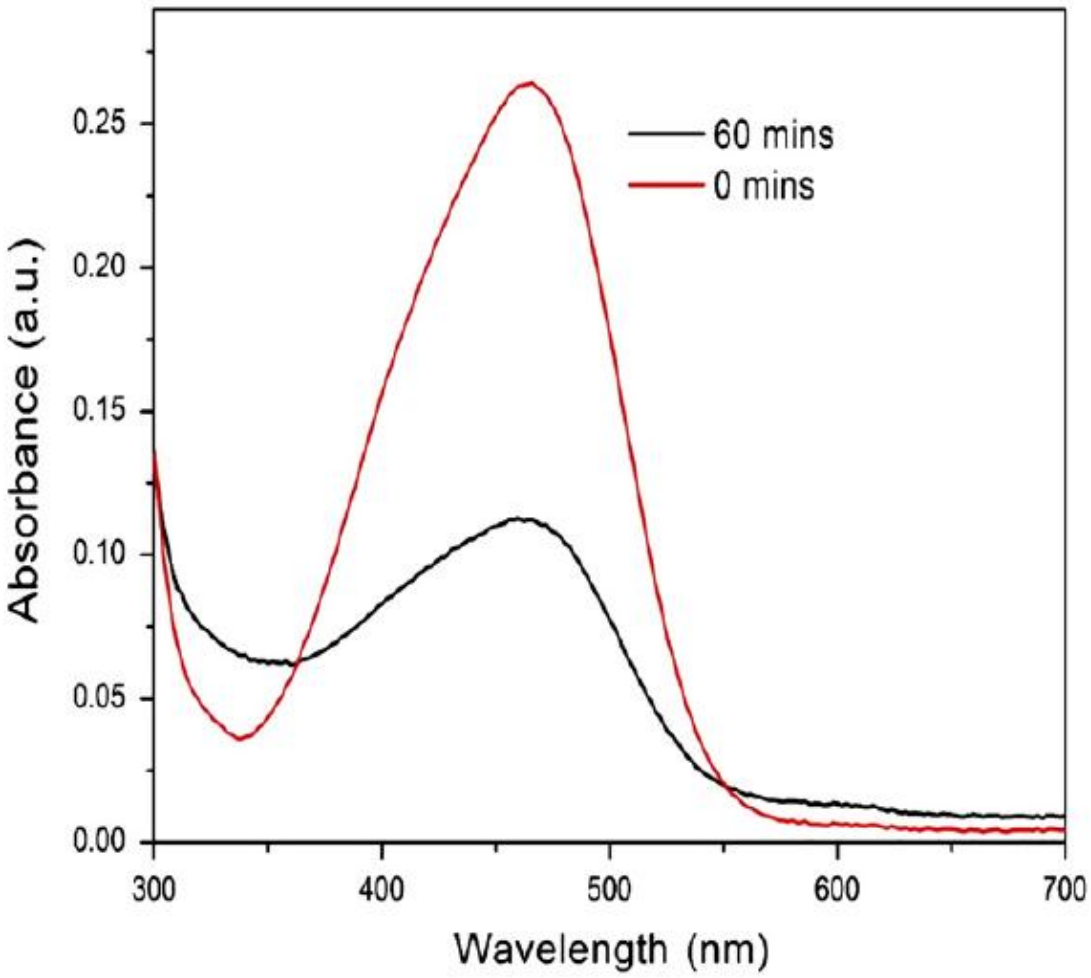
60 mins
0 mins
Absorbance (a.u.)
0.25
0.20
0.15
0.10
0.05
0.00
300
400
500
600
700
Wavelength (nm)

Fig. 8

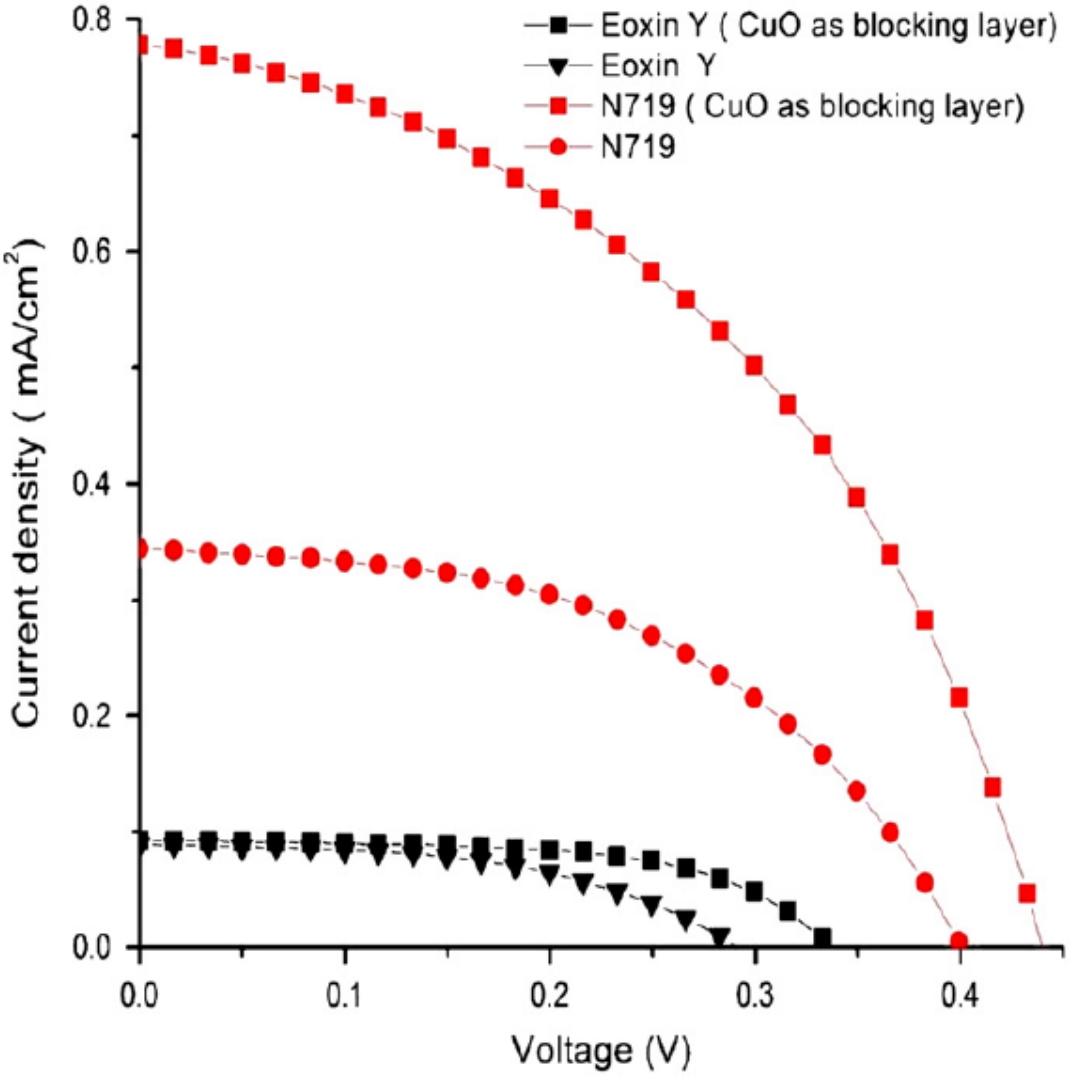
Eoxin Y (CuO as blocking layer)
Eoxin Y
N719 (CuO as blocking layer)
N719
Current density (mA/cm^2)
Voltage (V)
0.0
0.2
0.4
0.6
0.8
0.0
0.1
0.2
0.3
0.4

Fig. 9